HHS Public Access

Author manuscript

SLAS Technol. Author manuscript; available in PMC 2019 April 01.

Published in final edited form as:

SLAS Technol. 2018 April ; 23(2): 154–163. doi:10.1177/2472630317742071.

Embedded Multimaterial Extrusion Bioprinting

Marco Rocca[1,†], **Alessio Fragasso**[1,2,†], **Wanjun Liu**[1,3], **Marcel A. Heinrich**[1,4], and **Yu Shrike Zhang**[1]

[1]Division of Engineering in Medicine, Department of Medicine, Brigham and Women's Hospital, Harvard Medical School, Cambridge, MA, USA [2]Department of Bionanoscience, Kavli Institute of Nanoscience, Delft University of Technology, Delft, The Netherlands [3]Key Laboratory of Textile Science and Technology, College of Textiles, Donghua University, Shanghai, P.R. China [4]MIRA Institute of Biomedical Technology and Technical Medicine, Department of Developmental BioEngineering, University of Twente, Enschede, The Netherlands

Abstract

Embedded extrusion bioprinting allows for the generation of complex structures that otherwise cannot be achieved with conventional layer-by-layer deposition from the bottom, by overcoming the limits imposed by gravitational force. By taking advantage of a hydrogel bath, serving as a sacrificial printing environment, it is feasible to extrude a bioink in freeform until the entire structure is deposited and crosslinked. The bioprinted structure can be subsequently released from the supporting hydrogel and used for further applications. Combining this advanced three-dimensional (3D) bioprinting technique with a multimaterial extrusion printhead setup enables the fabrication of complex volumetric structures built from multiple bioinks. The work described in this paper focuses on the optimization of the experimental setup and proposes a workflow to automate the bioprinting process, resulting in a fast and efficient conversion of a virtual 3D model into a physical, extruded structure in freeform using the multimaterial embedded bioprinting system. It is anticipated that further development of this technology will likely lead to widespread applications in areas such as tissue engineering, pharmaceutical testing, and organs-on-chips.

Keywords

bioprinting; multimaterial; extrusion; embedded; freeform

Introduction

Bioprinting is an advanced biofabrication technology that allows for the generation of customized tissues and cell-laden structures aimed at improving current medical treatments.[1–3] So far, bioprinting has found two main applications. The first one intends to improve our

Corresponding Author: Yu Shrike Zhang, Division of Engineering in Medicine, Department of Medicine, Brigham and Women's Hospital, Harvard Medical School, 65 Landsdowne St., PRB 277, Cambridge, MA, 02139, USA. yszhang@research.bwh.harvard.edu.
[†]These authors contributed equally as the first author.

Declaration of Conflicting Interests

The authors declared no potential conflicts of interest with respect to the research, authorship, and/or publication of this article.

capability in the fabrication of human tissue and organ models, which provide structures and functionalities simulating their in vivo counterparts for use in drug screening.[4–7] Alternatively, bioprinted artificial tissues and organs can also be used for transplantation and regenerative medicine purposes to heal those that are injured or diseased in the human body.[8–11]

Bioprinting can be generally regarded as the computer-aided material patterning process for creating three-dimensional (3D) cell-laden structures with predefined shapes and compositions.[1,2,12,13] It usually involves programmed pattern generation using a hydrogel-based biomaterial, termed the bioink, which serves as the mimic of the extracellular matrix (ECM), to provide a suitable microenvironment for the cells to respond to.[1,2,14] Due to its strong potential in biomedical applications, this versatile technology has undergone rapid evolvement in the past decade, with many variations of the techniques developed, including laser-induced forward transfer (LIFT),[15–18] stereolithography,[19,20] inkjet bioprinting,[21–25] and extrusion bioprinting.[1,26–30] Among these, extrusion-based bioprinting is advantageous by enabling accurate, continuous, and fast deposition of the bioink at relatively low cost and system complexity.[31] Nonetheless, current extrusion bioprinting strategies still present limitations, in particular the generation of complex freeform 3D structures composed of multiple bioinks capable of self-supporting without deformation, at high fidelity.[12]

Here, we propose a solution that focuses on solving such technical limitations by developing a multimaterial embedded extrusion bioprinting process (Fig. 1).[12,32–35] The supporting hydrogel matrix relied on a thermoresponsive and biocompatible material, Pluronic F127 (PF-127), which presents a reversible sol-gel phase transition property at different temperatures due to the formation of micelle structures beyond the critical micelle temperature.[36,37] The literature has reported the use of a gelatin slurry, as well as a Carbopol granular medium, as the supporting bath, but PF-127, which is commonly utilized as a fugitive bioink,[38,39] has not been adopted for this purpose.[32,33]

On the other hand, alginate was used as the bioink due to its good biocompatibility, fast physical gelation, and low cost.[40] When extruded inside the PF-127 bath, the alginate bioink could be shaped into a freeform structure. To improve the mechanical stability of the extruded alginate structures, $CaCl_2$ was further mixed with the PF-127 bath to foster the ionic crosslinking of the bioink postbioprinting.[41] Upon complete solidification of alginate, PF-127 could be liquefied by cooling it down to 4°C, enabling the release and retrieval of the bioprinted freeform structure. The bioprinting apparatus, that is, the customized 3D bioprinter equipped with a multichannel, single-printhead pneumatic system, was previously described in our recent publication.[42] This article further describes the materials, hardware, and software developed to adapt the customized multimaterial setup to embedded bioprinting. For this purpose, an automated approach that allowed for rapid design, G-code generation, and bioprinting, along with specially designed printheads, was implemented and optimized to achieve multimaterial embedded extrusion bioprinting.

Materials and Methods

Bioprinter Software Interface

A standard commercially available 3D printer (Lulzbot TAZ 5 Lulzbot; Aleph Objects, Loveland, CO) was customized and used to carry out the experiments. Hardware and firmware modifications to achieve multimaterial extrusion bioprinting have been described in our previous report and will not be further elaborated.[42] Here, we present a fully automated 3D printing workflow for the generation of multimaterial structures by means of a CAD software, a G-code generator, and R programming (https://www.r-project.org). The software used to create the 3D models was SolidWorks (Concord, MA). Objects constituted by different materials were exported in the Additive Manufacturing File Format (AMF), which contained information not only of the model geometry, but also about the material.[43] The generated file was imported in Slic3r (https://www.slicer.org), a G-code generator software, to convert 3D multimaterial models into a sequence of specific commands readable by the 3D printer, that is, the G-code. The G-code is a text file containing instructions for the 3D printer, specifying the movements of the extruder in the *x-y-z* direction, together with its speed and the material to be extruded. However, the G-code generated by Slic3r is meant for a standard plastic extrusion printer. Therefore, a custom-written R script was used to further process the G-code to add and remove commands in a programmatic way, according to the needs of our customized bioprinting setup. In particular, changes were implemented to control the array of pneumatic valves, which were responsible for extrusion and switching among different bioinks. The additional functionalities were carefully synchronized with the movements of the printhead, taking into account the switching delay introduced by the actuation of the valves.

Extrusion Nozzle Design

Single-Nozzle Design—To fabricate the printhead, the parameters to be considered were (1) the inner diameter of the extruding needle to guarantee a fine resolution of the bioprinted structure without clogging the needle; (2) the stiffness of the needle, essential in providing a high resolution while preventing its bending caused by the friction against the hydrogel bath; and (3) the outer diameter of the nozzle, since if the nozzle shifts a large amount of hydrogel in the bath when moving, the recovery of PF-127 allowed by its thixotropic properties[44] would fail and air bubbles could be easily introduced, causing possible damage to the bioprinted structures.

Traditional printheads based on commercially sourced needles used for extrusion bioprinting cannot satisfy the challenges introduced by embedded bioprinting, and therefore to achieve an optimal trade-off between these parameters, a novel design of the extrusion printhead was developed. This new extrusion printhead was based on a telescopic structure, in which metal tubes with different diameters were combined to support the thin inner extrusion needle, keeping a high resolution, together with a good stiffness of the overall structure (Fig. 2A). The extrusion nozzle used in this case was composed of a 30G needle tip with an inner diameter of 159 μm and an outer diameter of 311 μm. The first-level supporting needle to provide more robustness to the tip needle had an inner diameter of 330 μm and an outer diameter of 635 μm. The supporting tube, which held the supporting needle, had an inner

diameter of 828 μm and an outer diameter of 1066 μm. Finally, the anchor tube used to fix the nozzle structure to the bioprinter had an inner diameter of 1194 μm and an outer diameter of 1651 μm. The bioink was delivered to the needle tip by means of a Teflon tube, with an outer diameter of 770 μm and an inner diameter of 300 μm.

Multinozzle Design—Previous cases of embedded bioprinting have led to long extrusion times due to the physical alternation of individual printheads during the deposition processes to achieve multimaterial embedded bioprinting.[45,47] In contrast, our novel multinozzle design could potentially allow for rapid multimaterial embedded extrusion.[42] To extrude different bioinks from the same printhead, the main issue that should be addressed is to avoid different materials coming into contact with each other prior to extrusion and to prevent the intermixing of different materials. This prerequisite leads to the necessity of having multiple nozzle tips in a single printhead, one for each material (Fig. 2B, C). To design this structure, three needles were attached together to form a stiff but small tip. To maintain a robust needle structure, an approach similar to that of the telescopic single-nozzle design was applied, resizing the encasing tubes accordingly. The multinozzle printhead consisted of three 27G needles with an inner diameter of 210 μm and an outer diameter of 413 μm packed against each other sideways. The first-level supporting needle, which contained all three inner needles, had an inner diameter of 965 μm and an outer diameter of 1270 μm. The supporting tube had an inner diameter of 1321 μm and an outer diameter of 1575 μm. Finally, the anchor tube possessed an inner diameter of 1600 μm and an outer diameter of 2108 μm. The Teflon tubes used to deliver the bioink to the anchor tube were the same as those for the single-nozzle printheads and had an outer diameter of 770 μm and an inner diameter of 300 μm.

Chemical Optimization for Embedded Bioprinting

Preparation of the Bioink—A stock of 4% alginate (w/v; Sigma-Aldrich, St. Louis, MO) in deionized (DI) water was prepared and stored at 4°C. The ideal concentration of alginate to allow for an optimal extrusion had been measured experimentally to be between 1.5% and 2.5%. Therefore, for all the experiments performed in this work, 2% alginate was used. From the stock of 4% alginate, a solution of 2% was prepared by diluting the stock with DI water. When necessary, fluorescent beads (AmeriColor, Placentia, CA) were added to the 2% alginate solution to enhance the visibility of the bioprinted structure under UV light.

Preparation of the Supporting Bath—The supporting hydrogel bath was prepared by dissolving PF-127 (Sigma-Aldrich) in DI water. Since PF-127 undergoes sol-gel transition at room temperature, the solution was initially maintained at 4°C to avoid gelation. Next, $CaCl_2$ was added to the PF-127 solution from a previously prepared stock at 2% (w/v) to obtain a final concentration of 0.05% $CaCl_2$ in the PF-127 solution. $CaCl_2$ is the crosslinking agent for alginate, and its presence is essential in the optimized bioprinting conditions.

The supporting hydrogel with a total volume of 300 mL was placed in a glass container (10 × 10 × 5 cm^3 in size), and studies were performed to optimize the PF-127 concentration (Fig. 3). PF-127 solutions at different concentrations (21%–30% [w/v]) could all

successfully gel when placed at 37°C for varying time periods (Fig. 3A). The curing temperature of 37°C was chosen as such to provide a suitable environment for future studies involving cells. Liquefaction of the PF-127 baths (10%–30% [w/v]) was then measured, where all gelled samples (1 h at 37°C) were placed back at room temperature (23°C) and the transition time from gel to liquid was measured (Fig. 3B). It was observed that only the samples at concentrations of ≤20% were liquefied at room temperature; on the contrary, all the other samples at concentrations of >20% were still in the hydrogel state, and hence they were not included in the graph, as we did not observe any liquefaction for those PF-127 hydrogels. Since our bioprinting times rarely exceeded 200 min, PF-127 at concentrations of >20% would have provided sufficient mechanical stability over the time periods required for bioprinting, and hence they could be safely used as supporting hydrogel without the need for altering the ambient environment.

Therefore, PF-127 at the concentration of 23% was chosen, as it provided a good trade-off to allow relatively fast gelation time and stability at room temperature, avoiding phase transition of the supporting bath during the bioprinting process. We then fine-tuned its optimal curing time via iterative qualitative assessment, and a gelation time of 27 min for PF-127 at this concentration was determined. We generally observed that for shorter times, the alginate spread into the supporting hydrogel, while for longer times the printhead was constantly bent when moving inside the hydrogel bath due to the high viscosity of the hydrogel.

After the structure was bioprinted, a resting period of 30 min was measured to further allow the alginate to fully crosslink in the PF-127-$CaCl_2$ hydrogel bath. The extraction of the structure from the PF-127 hydrogel could be achieved upon its liquefaction at 4°C for varying periods.

Results

Single-Material Embedded Extrusion Bioprinting

The initial experiments were carried out using the designed coaxial single-material printhead to optimize our 3D bioprinting system prior to proceeding to the multimaterial extrusion processes. The bioprinting conditions for single-material extrusion were first optimized against parameters such as the pressure applied to extrude the bioink, the speed of motion of the printhead, and the interline spacing. The resulting structures were characterized and assessed to extract the optimal bioprinting conditions. The pattern used for this purpose was an array of 10 lines, each extruded in the PF-127 hydrogel bath at a different speed. The same analysis was repeated at varying extrusion pressures. The samples were analyzed with fluorescence microscopy, and the average diameters of the lines were calculated and plotted depending on the extrusion pressure (Fig. 4). The results showed that a resolution of 50–100 μm was potentially achievable with different extrusion pressures.

Next, we tested the mechanical properties of bioprinted cylindrical objects with different interline spacing (Fig. 5). Different columns compared the Young's moduli, extracted from the slopes in the linear parts of the stress–strain curves obtained from the mechanical testing data, of cylinders bioprinted with an equally varying interline spacing in the *x*-*y*-*z* direction.

A high Young's modulus was found for bioprinted constructs with interline spacing of 250 and 300 μm. This observation could be related to the amount of bioink extruded per unit volume. If the interline spacing is too large, there would be gaps between the alginate lines, which could then be filled by PF-127 in the hydrogel bath. During the extraction process, PF-127 is removed and therefore the gaps will collapse, leading to a less compact structure. On the other hand, if the interline spacing is too small, there would be more alginate extruded in the available volume. This could lead to the spreading of the alginate outside of the bioprinted contours, which in turn lowers the resolution and creates inhomogeneity in the structure with compromised mechanics. Optimal values for pressure, speed, and interline spacing were accordingly set to 20 psi, 10 mm/s, and 300 μm, respectively, to obtain satisfactory bioprinting of single-material structures.

Subsequently, 3D models characterized by increasing geometrical complexity were designed using SolidWorks and bioprinted with a single-material printhead. A UV lamp was employed to visualize the bioprinted structures, and photographs were taken with a digital single-lens reflex camera. Initially, objects such as a cube and a cartoon of the heart were generated (Fig. 6A,B). During the deposition, issues related to alginate spreading were encountered when changing the location of extrusion, leading to diffusion of alginate inside the PF-127 bath into the surroundings of the point of interest, hence limiting the structural fidelity of the final objects. This was mainly due to the fact that the continuous extrusion process caused overdispensing of the bioink.[42] To compensate for this limitation, the G-code was processed by the custom-written R script. As such, the improved system allowed us to suspend the flow when the printhead was relocated from one point to another, avoiding unnecessary dispensing during this process. Having this full control over the actuation of the valves enabled us to further fabricate more complex freeform alginate constructs. In particular, freestanding objects, such as the MIT letters, a Mobius strip, and a Klein bottle, were readily bioprinted (Fig. 6C–I).

Ultimately, bioprinting aims at creating organ-mimetic cell-laden constructs.[1] Therefore, the capability of our bioprinting system to reproduce biologically relevant organlike structures was further demonstrated. 3D human heart- and kidney-like objects composed of several tens of layers of alginate could be successfully produced by employing optimized embedded extrusion conditions (Fig. 6J–L). Each structure was bioprinted individually within a time span ranging from tens of minutes to a couple hours, depending on its size and complexity. For example, to bioprint a mimic of the human heart with an estimated volume of ~1.5 cm^3, it took 2 h 15 min using the bioprinting settings at a relatively high resolution (300 μm in the *x*-*y*-*z* directions).

Multimaterial Embedded Extrusion Bioprinting

After optimizing the parameters for single-material embedded extrusion bioprinting, we subsequently investigated the possibility of achieving the deposition of multiple bioinks in freeform during the same bioprinting process in an effective manner.[45,46] This technique will potentially pave the avenue to the fabrication of 3D tissues laden with different cell types, which is a critical step toward the improvement of tissue biofabrication in regenerative medicine and organ model generation. So far, advanced 3D bioprinters have allowed the

extrusion of different bioinks using systems consisting of multiple printheads, each of them allowing for the extrusion of only one single material.[47] Our goal is to develop a single printhead containing several printheads, each connected to its own bioink reservoir. This could allow for a faster, more accessible, and lower-cost approach to multimaterial extrusion, which is more advantageous than the multiprinthead extrusion setup. While a similar design of such a single-printhead multimaterial system was recently reported by us, [42] here we further optimized it specifically for embedded bioprinting.

Multimaterial bioprinting was achieved through optimizations in the software/hardware setup, as well as in chemical conditions. A continuous switching between the materials based on the needle position in the 3D space could be achieved (Fig. 7A–C). The transition between the materials could be completed within a few hundred micrometers. This spatial resolution could potentially be further lowered to below 300 μm through the manipulation of the pneumatic pressure to ensure a sharp transition and separation between the consecutively extruded materials. It should be noted that our studies on the multimaterial setup have been conducted using only one single material, that is, 2% alginate, colored with different dyes. The main reason for this was to keep the bioink properties constant to detect and isolate errors during our optimization processes. The extrusion of several materials with different rheological properties, as well as crosslinking processes in this case, would inevitably introduce further complications, and thus has not been pursued in the current work. As such, a multimaterial pattern was successfully bioprinted on a glass slide, highlighting the improvements at the software and hardware levels to manage the extrusion of different materials (Fig. 7D). In our software design, the 3D model was created by retaining each material to be extruded as an individual entity, indicating that the G-code generator was programmed to recognize the different colors (i.e., subparts with different materials) in the model and assign them to specific nozzles in an automated manner, contrary to the manual adjustments needed in our original report.[42] A modification of the G-code generator was also implemented to adapt the G-code to the extrusion of hydrogel bioinks, instead of the plastics used in the original 3D printer. We were able to prove our ability to further bioprint complex multimaterial structures in freeform (Fig. 7E–H), using the optimized hardware/software combinations with the extrusion system. The injection of air bubbles into the structures during the bioprinting process could be a major issue affecting the integrity of the extruded objects, which was controlled by the use of an optimized supporting PF-127 hydrogel bath and by properly tuning the movement speed of the printhead.

Discussions

We have demonstrated the ability to achieve the fabrication of multimaterial structures using an automated 3D embedded extrusion bioprinting technique. So far, fabrication of freeform structures constituting several materials has been largely prohibitive. For example, in a previous report by us, while the concept of single-printhead design to achieve continuous multimaterial extrusion bioprinting was proposed, it was mainly used to deposit planar or simple 3D shapes and was not optimized for the generation of freeform structures.[42] Recent efforts have succeeded in the development of embedded bioprinting to create freeform objects using a supporting hydrogel bath that can be selectively removed postbioprinting. [33,42] We have provided here a proof-of-concept demonstration, showing that the

combination of embedded bioprinting with single-printhead multimaterial extrusion bioprinting was possible to fabricate various complex 3D structures in freeform, using an automation process involving both hardware and software optimizations. Our results proved that freeform macroscopic objects with biologically relevant conformations could be realized with micrometric accuracy.

We further emphasize the accessibility and efficiency of our technique, based on commercially available software and hardware, customized and automated for our purpose. We estimated a deposition speed that is 4–15 times faster than that of other multimaterial setups based on separate printheads to achieve embedded bioprinting,[35,42,45,47] while maintaining a low cost of the total system without significantly increased complexity in the printhead fabrication. Nevertheless, issues concerning the damage of the structure during extraction from the liquefied PF-127 bath could still affect the mechanical stability of the retrieved objects. Particular attention also has to be paid at critical locations during extrusion, such as the interfaces between different materials and the turns of sharp corners. Moreover, the possibility of independently tuning the flow rates of the different bioinks, not implemented in the current setup, would help to distribute them more evenly. This strategy could mitigate the effect of the difference in viscosity of the bioinks and eliminate over- or underdispensing, which might cause the final structure to present inhomogeneity and mechanical instability. Further studies will explore the possibility of using other bioinks besides alginate to improve the biocompatibility without affecting the mechanical properties of the outcoming structure. A mixture of alginate and GelMA is a promising candidate to achieve this goal.[42] Lastly, PF-127 supporting hydrogels constituted in more physiologically relevant media (e.g., saline and serum) will also be explored and optimized to eventually achieve multimaterial cell bioprinting.

Conclusions

We have reported on the development of a multimaterial embedded bioprinting process based on optimizations in the software, hardware, and materials. It is believed that further improvements of this technology will contribute to our enhanced capability to fabricate complex viable cell-laden structures to reproduce tissue and organ functionality, potentially leading to widespread applications ranging from biomedicine and bioelectronics to smart materials for use in home, energy, and the environment.

Acknowledgments

The authors acknowledge funding from the National Cancer Institute of the National Institutes of Health (K99CA201603), the Lush Prize, and the Science and Technology Commission of Shanghai Municipality (STCSM) 17JC 1400200.

Funding

The authors received no financial support for the research, authorship, and/or publication of this article.

References

1. Murphy SV, Atala A. 3D Bioprinting of Tissues and Organs. Nat Biotechnol. 2014; 32(8):773–785. [PubMed: 25093879]

2. Dababneh AB, Ozbolat IT. Bioprinting Technology: A Current State-of-the-Art Review. J Manuf Sci Eng. 2014; 136(6):061016.

3. Groll J, Boland T, Blunk T, et al. Biofabrication: Reappraising the Definition of an Evolving Field. Biofabrication. 2016; 8(1):013001. [PubMed: 26744832]

4. Hyungseok L, Dong-Woo C. One-Step Fabrication of an Organ-on-a-Chip with Spatial Heterogeneity Using a 3D Bioprinting Technology. Lab Chip. 2016; 16:2618–2625. [PubMed: 27302471]

5. Huh D, Matthews BD, Mammoto A, et al. Reconstituting Organ-Level Lung Functions on a Chip. Science. 2010; 328:1662–1668. [PubMed: 20576885]

6. Sonntag F, Schilling N, Mader K, et al. Design and Prototyping of a Chip-Based Multi-Micro-Organoid Culture System for Substance Testing, Predictive to Human (Substance) Exposure. J Biotechnol. 2010; 148:70–75. [PubMed: 20138930]

7. Gunther A, Yasotharan S, Vagaon A, et al. A Microfluidic Platform for Probing Small Artery Structure and Function. Lab Chip. 2010; 10:2341–2349. [PubMed: 20603685]

8. Collins SF. Bioprinting Is Changing Regenerative Medicine Forever. Stem Cells Dev. 2014; 1:79–82.

9. Skardal A, Mack D, Kapetanovic E, et al. Bioprinted Amniotic Fluid-Derived Stem Cells Accelerate Healing of Large Skin Wounds. Stem Cells Transl Med. 2012; 1:792–802. [PubMed: 23197691]

10. Cui X, Breitenkamp K, Finn MG, et al. Direct Human Cartilage Repair Using Three-Dimensional Bioprinting Technology. Tissue Eng Part A. 2012; 18:1304–1312. [PubMed: 22394017]

11. Munoz-Abraham AS, Rodriguez-Davalos MI, Bertacco A, et al. 3D Printing of Organs for Transplantation: Where Are We and Where Are We Heading? Curr Transpl Rep. 2016; 3(1):93–99.

12. De Maria C, Vozzi G, Moroni L. Multimaterial, Heterogeneous, and Multicellular Three-Dimensional Bioprinting. MRS Bullet. 2017; 42(8):578–584.

13. Guillemot F, Mironov V, Nakamura M. Bioprinting Is Coming of Age: Report from the International Conference on Bioprinting and Biofabrication in Bordeaux. Biofabrication. 2010; 2(1):1–7.

14. Maria, DeC, De Acutis, A., Carrabba, M., et al. Machine Design for Multimaterial Processing. In: Grumezescu, A., editor. Nanobiomaterials in Soft Tissue Engineering: Applications of Nanobiomaterials. Elsevier; Amsterdam: 2016. p. 111-140.

15. Schiele NR, Koppes RA, Corr DT. Laser Direct Writing of Combinatorial Libraries of Idealized Cellular Constructs: Biomedical Applications. Appl Surf Sci. 2009; 255(19):5444–5447.

16. Colina M, Serra P, Fernandez-Pradas JM, et al. DNA Deposition through Laser Induced Forward Transfer. Biosens Bioelectron. 2005; 20:1638–1642. [PubMed: 15626620]

17. Ringeisen BR, Kim H, Barron JA, et al. Laser Printing of Pluripotent Embryonal Carcinoma Cells. Tissue Eng. 2004; 10:483–491. [PubMed: 15165465]

18. Guillemot F, Souquet A, Catros S, et al. Laser-Assisted Cell Printing: Principle, Physical Parameters versus Cell Fate and Perspectives in Tissue Engineering. Nanomedicine. 2010; 5:507–515. [PubMed: 20394540]

19. Wang Z, Abdulla R, Parker B. A Simple and High-Resolution Stereolithography-Based 3D Bioprinting System Using Visible Light Crosslinkable Bioinks. Biofabrication. 2015; 7(4):1–29.

20. Dhariwala B, Hunt E, Boland T. Rapid Prototyping of Tissue-Engineering Constructs, Using Photopolymerizable Hydrogels and Stereolithography. Great Lakes Biomed Conf. 2004; 10(9): 1316–1322.

21. Nishiyama Y. Development of a Three-Dimensional Bioprinter: Construction of Cell Supporting Structures Using Hydrogel and State-of-the-Art Inkjet Technology. J Biomech Eng. 2009; 131(3): 035001. [PubMed: 19154078]

22. Saunders RE, Gough JE, Derby B. Delivery of Human Fibroblast Cells by Piezoelectric Drop-on-Demand Inkjet Printing. Biomaterials. 2008; 29:193–203. [PubMed: 17936351]

23. Xu T, Gregory CA, Molnar P, et al. Viability and Electrophysiology of Neural Cell Structures Generated by the Inkjet Printing Method. Biomaterials. 2006; 27:3580–3588. [PubMed: 16516288]

24. Phillippi JA, Miller E, Weiss L, et al. Microenvironments Engineered by Inkjet Bioprinting Spatially Direct Adult Stem Cells toward Muscle- and Bone-Like Subpopulations. Stem Cells. 2008; 26:127–134. [PubMed: 17901398]
25. Nakamura M, Kobayashi A, Takagi F, et al. Biocompatible Inkjet Printing Technique for Designed Seeding of Individual Living Cells. Tissue Eng. 2005; 11:1658–1666. [PubMed: 16411811]
26. Iwami K, Noda T, Ishida K, et al. Bio Rapid Prototyping by Extruding/Aspirating/Refilling Thermoreversible Hydrogel. Biofabrication. 2010; 2:014108. [PubMed: 20811123]
27. Shor L, Güçeri S, Chang R, et al. Precision Extruding Deposition (PED) Fabrication of Polycaprolactone (PCL) Scaffolds for Bone Tissue Engineering. Biofabrication. 2009; 1:015003. [PubMed: 20811098]
28. Zhang YS, Yue K, Aleman J, et al. 3D Bioprinting for Tissue and Organ Fabrication. Ann Biomed Eng. 2017; 45(1):148–163. [PubMed: 27126775]
29. Zhang YS, Duchamp M, Oklu R, et al. Bioprinting the Cancer Microenvironment. ACS Biomater Sci Eng. 2016; 2(10):1710–1721. [PubMed: 28251176]
30. Cohen DL, Malone E, Lipson H, et al. Direct Freeform Fabrication of Seeded Hydrogels in Arbitrary Geometries. Tissue Eng. 2006; 12:1325–1335. [PubMed: 16771645]
31. Reid JA, Mollica PA, Sachs PC. Accessible Bioprinting: Adaptation of a Low-Cost 3D-Printer for Precise Cell Placement and Stem Cell Differentiation. Biofabrication. 2016; 8(2):025017. [PubMed: 27271208]
32. Bhattacharjee T, Zehnder SM, Angelini TE. Writing in the Granular Gel Medium. Sci Adv. 2015; 1(8):e1500655. [PubMed: 26601274]
33. Hinton TJ, Jallerat Q, Feinberg AW. Three-Dimensional Printing of Complex Biological Structures by Freeform Reversible Embedding of Suspended Hydrogels. Sci Adv. 2015; 1(9):e1500758. [PubMed: 26601312]
34. Vozzi G, Tirella A, Ahluwalia A. Rapid Prototyping Composite and Complex Scaffolds with PAM2. Methods Mol Biol. 2012; 868:57–69. [PubMed: 22692604]
35. Highley CB, Rodell CB, Burdick JA. Direct 3D Printing of Shear-Thinning Hydrogels into Self-Healing Hydrogels. Adv Mater. 2015; 27:5075–5079. [PubMed: 26177925]
36. Mortensen K. PEO-Related Block Copolymer Surfactants. Colloids Surf. 2001; 185:277–292.
37. Bohorquez M, Koch C, Trygstad T, et al. A Study of the Temperature-Dependent Micellization of Pluronic F127. J Colloid Interface Sci. 1999; 216(1):34–40. [PubMed: 10395759]
38. Kolesky DB, Homan KA, Skylar-Scott MA, Lewis JA. Three-Dimensional Bioprinting of Thick Vascularized Tissues. Proc Natl Acad Sci USA. 2016; 113(12):3179–3184. [PubMed: 26951646]
39. Kolesky DB, Truby RL, Gladman AS, Busbee TA, Homan KA, Lewis JA. 3D Bioprinting of Vascularized, Heterogeneous Cell-Laden Tissue Constructs. Adv Mater. 2014; 26:3124–3130. [PubMed: 24550124]
40. Ozbolat IT, Hospodiuk M. Current Advances and Future Perspectives in Extrusion-Based Bioprinting. Biomaterials. 2015; 76:321–343. [PubMed: 26561931]
41. Kuo CK, Ma PX. Ionically Crosslinked Alginate Hydrogels as Scaffolds for Tissue Engineering: Part 1. Structure, Gelation Rate and Mechanical Properties. Biomaterials. 2001; 22(6):511–521. [PubMed: 11219714]
42. Liu W, Zhang YS, Heinrich M, et al. Rapid Continuous Multimaterial Extrusion Bioprinting. Adv Mater. 2017; 29:1604630.
43. Hiller JD, Lipson H. STL 2.0: A Proposal for a Universal Multi-Material Additive Manufacturing File Format. Solid Freeform Fabr Symp Proc. 2009:266–278.
44. Escobar-Chávez JJ, López-Cervantes M, Ganem-Quintanar A. Applications of Thermo- Reversible Pluronic F-127 Gels in Pharmaceutical Formulations. J Pharm Pharmaceut Sci. 2006; 9(3):339–358.
45. Khalil S, Nam J, Sun W. Multi-Nozzle Deposition for Construction of 3D Biopolymer Tissue Scaffolds. Rapid Prototyp J. 2005; 11(1):9–17.
46. Kang H, Lee SJ, Ko IK. A 3D Bioprinting System to Produce Human-Scale Tissue Constructs with Structural Integrity. Nat Biotechnol. 2016; 34(3):312–319. [PubMed: 26878319]

47. Ozbolat IT, Chen H, Yu Y. Development of ‘Multi-Arm Bioprinter’ for Hybrid Biofabrication of Tissue Engineering Constructs. Robot Comput Integr Manuf. 2014; 30(3):295–304.

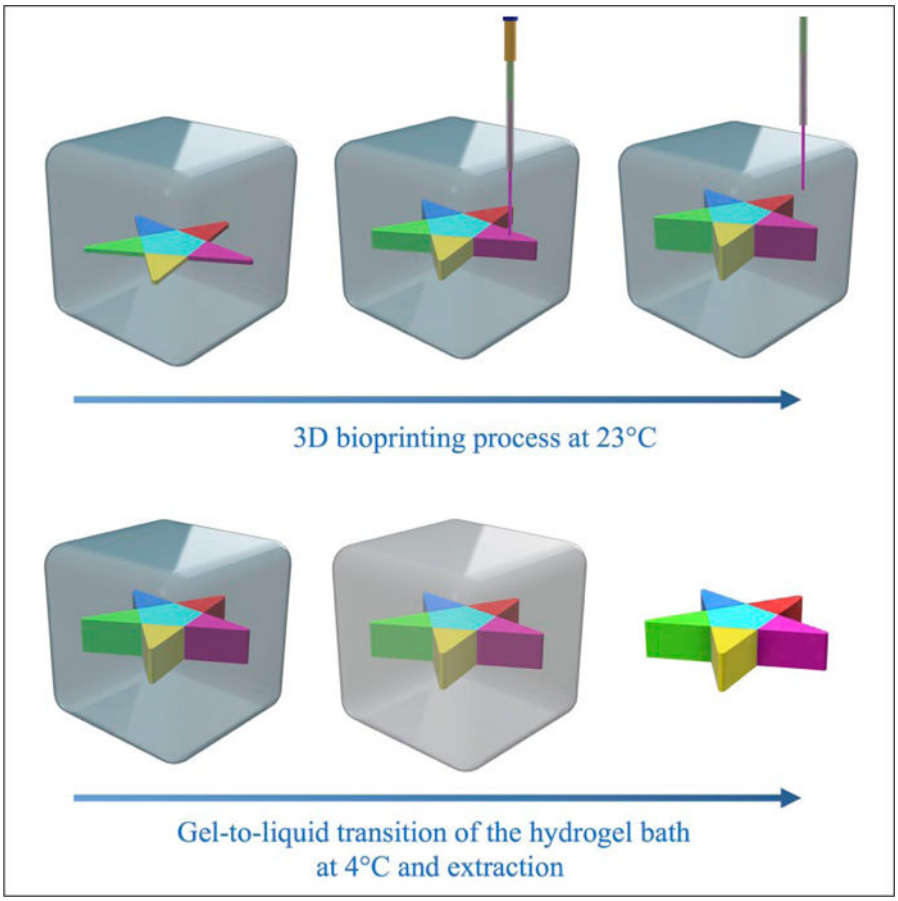

Figure 1.

Concept of the embedded multimaterial 3D bioprinting. Top: A custom-designed multinozzle printhead is used to deposit different bioinks into the supporting hydrogel bath, PF-127. The bioprinting process occurs at room temperature (23°C), after the PF-127 bath has formed a stable hydrogel bath. Bottom: To release the bioprinted structure, the supporting PF-127 hydrogel bath is cooled down to 4°C, hence inducing its gel-to-liquid transition and subsequent retrieval of the structure.

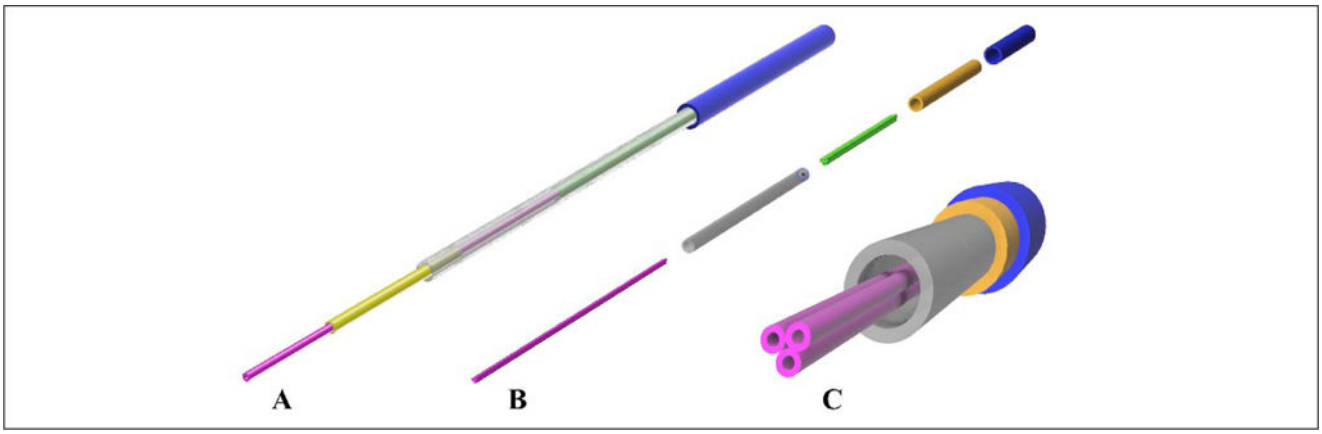

Figure 2.

(**A**) Design of the single-nozzle printhead. A thin tip (30G) with an inner diameter of 159 μm was encased in increasingly larger metal tubes to maintain a small nozzle size at the tip while at the same time keeping a stiff and rigid overall structure. (**B**) Exploded view of the design of a multinozzle printhead. Three thin tips (30G) were fixed together to form the extrusion nozzle. This allowed for different materials to be extruded simultaneously or sequentially, while avoiding intermixing of the hydrogels prior to extrusion. Similar to the single-nozzle approach, a sequence of three metal tubes with increasing diameters were used to make the structure stiffer and avoid its bending. (**C**) Front view of the multinozzle printhead.

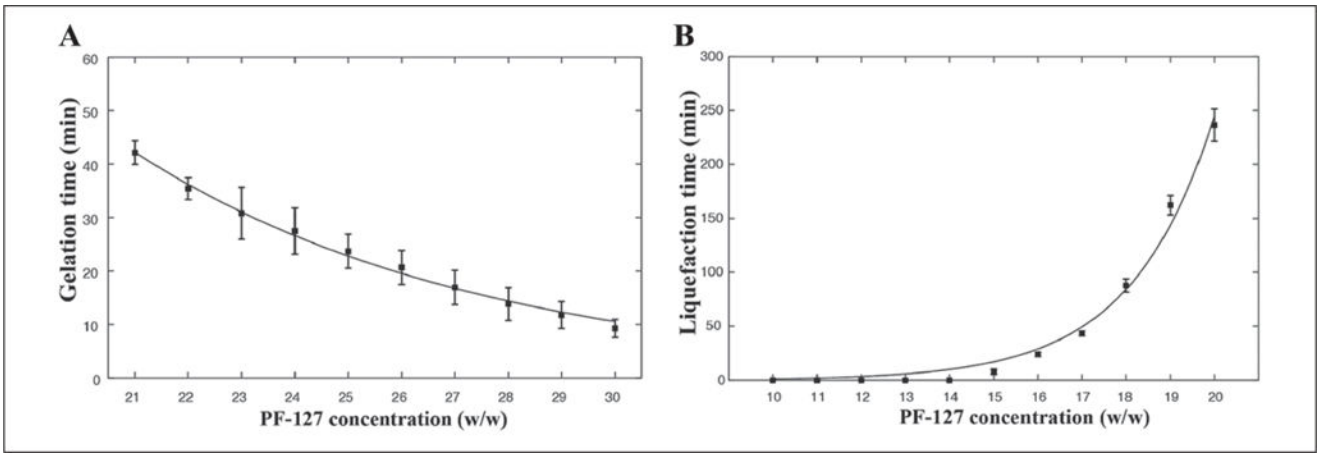

Figure 3.

Plots showing (**A**) gelation time and (**B**) liquefaction time vs. PF-127 concentration. (**A**) Gelation of PF-127 solutions at different concentrations of 21%–30%. The liquid solutions initially at 4°C were placed at 37°C until gelation was observed. (**B**) Liquefaction of PF-127 hydrogels at different concentrations of 10%–30%. The gelled samples were maintained at room temperature (23°C) for 12 h to observe if they could reach the liquid phase. All samples at concentrations of >20% did not show any liquefaction and hence were not included in the graph.

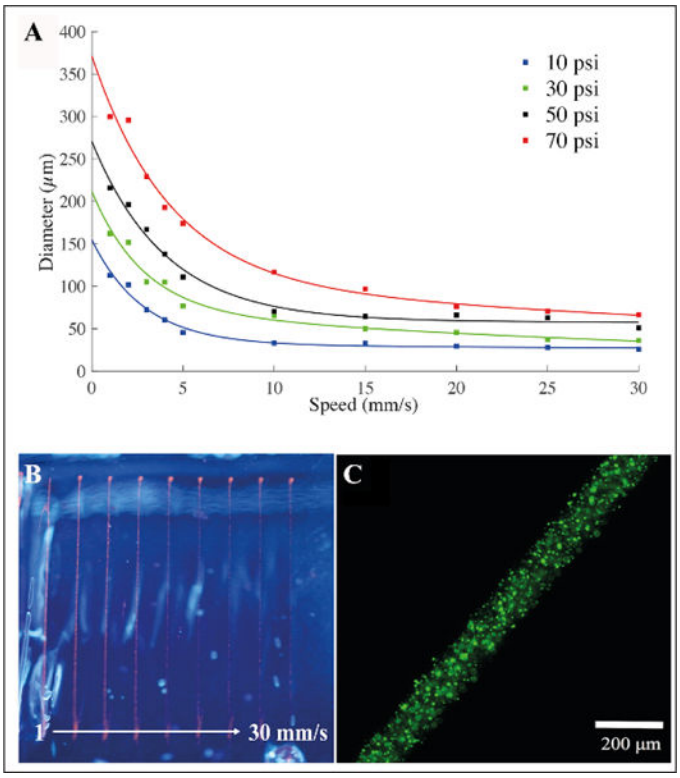

Figure 4.

Characterization of the filament diameter vs. nozzle speed and pressure. (**A**) Patterns consisting of 10 straight lines each with a different nozzle moving speed ranging from 1 to 30 mm/s were bioprinted inside the PF-127 supporting hydrogel bath. The same patterns were bioprinted again for different pressures, from 10 to 70 psi. (**B**) Top view of the alginate lines bioprinted inside the PF-127 bath at a speed of 1 up to 30 mm/s at 50 psi. (**C**) Fluorescence micrograph showing a line bioprinted at 70 psi and 5 mm/s.

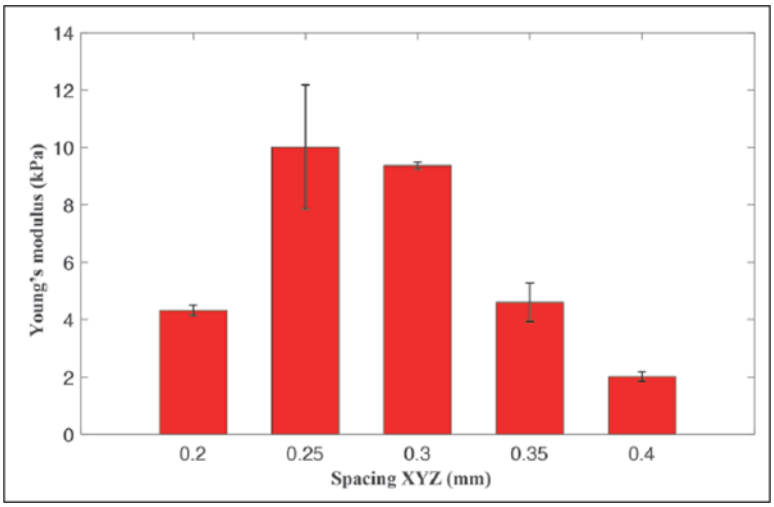

Figure 5.

Young's moduli of a series of bioprinted cylindrical structures at different interline spacing, equally varied along the *x, y*, and *z* directions.

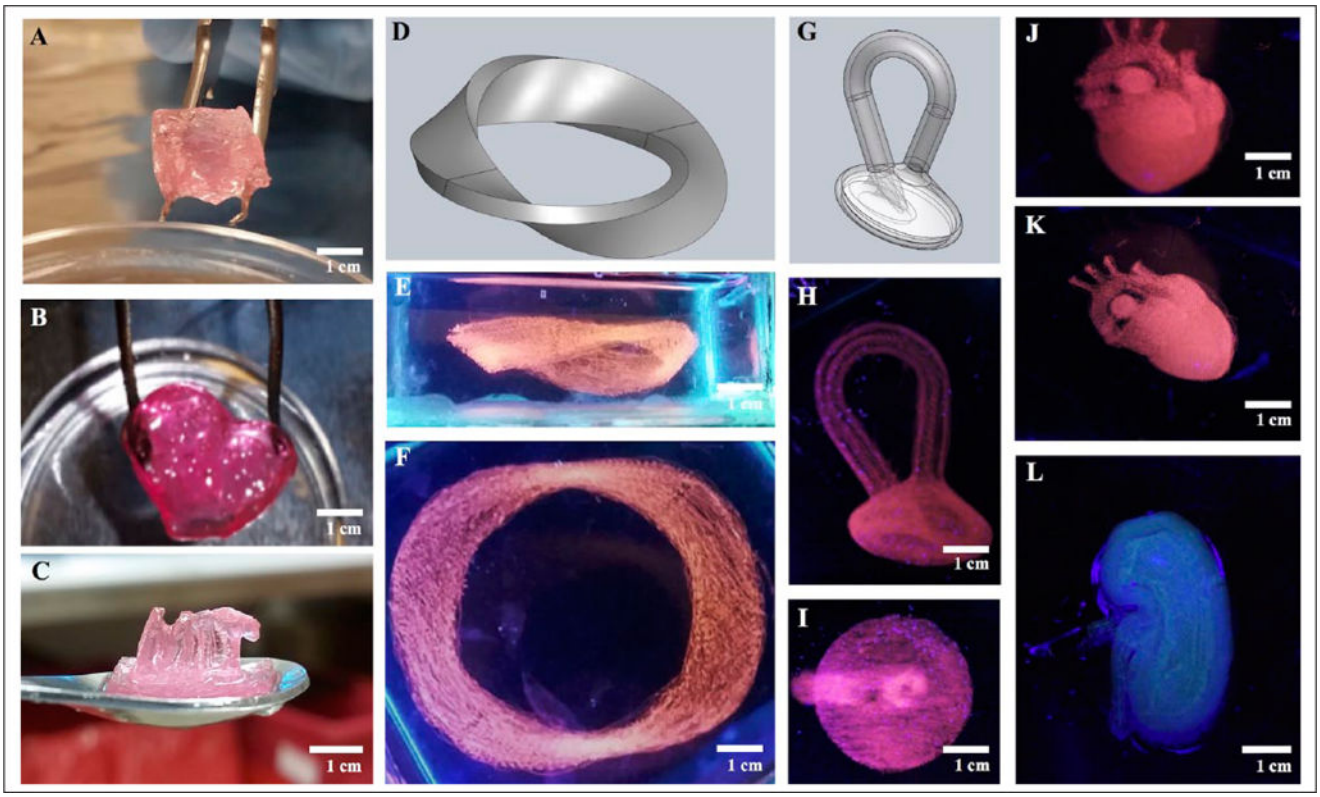

Figure 6.

Embedded bioprinting of single-material constructs. (**A–C**) Photographs showing (**A**) a cube, (**B**) a heart cartoon, and (**C**) MIT letters, indicating that the structures were sufficiently stiff to be extracted from the supporting bath and were able to self-support their weights. (**D–I**) Models and photographs showing (**D–F**) a Mobius strip and (**G–I**) a Klein bottle, proving that complex shapes that would conventionally require supporting pillars in normal extrusion 3D bioprinting methods could be readily achieved using embedded bioprinting. (**J–L**) Photographs showing (**J,K**) a heart-like structure and (**L**) a kidney-like structure, demonstrating that more complex macroscopic structures mimicking human organs could be bioprinted and have their shapes maintained after extraction from the sacrificial hydrogel bath.

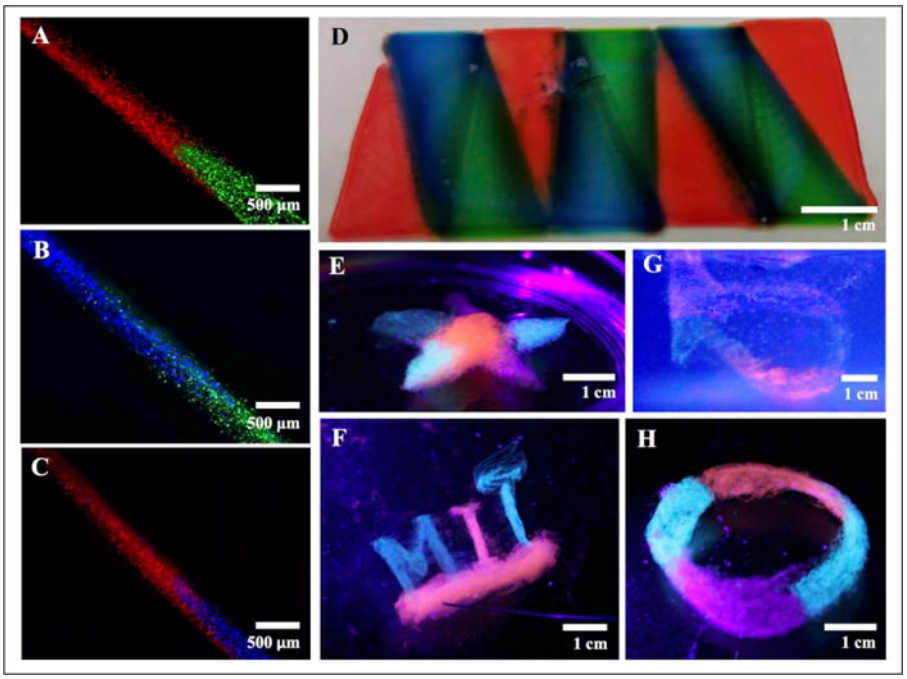

Figure 7.

Embedded bioprinting of multimaterial constructs. (**A–C**) Photographs showing the switching test for the multinozzle printhead. Alginate doped with three different dyes was used to visualize the switch between the different extrusion nozzles in a single printhead. (**D**) Photograph showing a structure with three alternating materials bioprinted on a glass slide. (**E–H**) Photographs showing embedded bioprinting of complex patterns containing multiple materials, including (**E**) a star, (**F**) MIT letters, (**G**) a Klein bottle, and (**H**) a Mobius strip.